nature photonics

FOCUS | REVIEW ARTICLE

PUBLISHED ONLINE: 27 NOVEMBER 2014 | DOI: 10.1038/NPHOTON.2010.285

Mapping nanoscale light fields

N. Rotenberg and L. Kuipers*

The control of light fields on subwavelength scales in nanophotonic structures has become ubiquitous, driven by both curiosity and a multitude of applications in fields ranging from biosensing to quantum optics. Mapping these fields in detail is crucial, as theoretical modelling is far from trivial and highly dependent on nanoscale geometry. Recent developments of nanoscale field mapping, particularly with near-field microscopy, have not only led to a vastly increased resolution, but have also resulted in increased functionality. The phase and amplitude of different vector components of both the electric and magnetic fields are now accessible, as is the ultrafast temporal or spectral evolution of propagating pulses in nanostructures. In this Review we assess the current state-of-the-art of subwavelength light mapping, highlighting the new science and nanostructures that have subsequently become accessible.

Near-field microscopy is a powerful tool that allows the study of the complex electromagnetic fields that surround nanophotonic structures. As our control over the feature size of these structures becomes ever finer, the ability to image their near fields becomes ever more crucial. This is because, at the nanoscale, light–matter interactions are intimately linked to an object's geometry and not just to the optical properties of its constituent materials. Consequently, near-field mappings are often the only route to understanding the underlying physical processes of exciting phenomena such as extraordinary optical transmission[1,2], light propagation through photonic crystal waveguides[3,4], and the optical response of nanoantennas[5,6]. Likewise, when accurate knowledge of the details of nanoscopic light fields is crucial to the performance of a device, near-field imaging becomes essential. Examples of such situations include the creation of hotspots for nonlinear nanophotonics[7] or sensing applications[8], the way in which nanophotonic structures direct light flow[9], or the generation of structured fields for nanomanipulation[10,11]. In all, there are a host of fields that stand to gain from the information available from near-field microscopy.

In this Review we discuss recent progress towards a complete mapping of light fields at the nanoscale, suggesting new scientific avenues that are opened by these advances. We begin by briefly reviewing the basics of subwavelength field mapping. We then outline recent progress in the mapping of electric near-field vector components, and progress to mapping that goes beyond the vector nature, such as time- or frequency-resolved measurements. We then address recent progress towards the mapping of magnetic near fields, and in particular towards the ability to simultaneously map the entire electromagnetic near field. Throughout the entire Review, we highlight exciting nanophotonic systems whose near fields can be accessed because of progress in this field. Lastly, we end with a brief outlook on the remaining challenges in the pursuit of a complete nanoscale near-field mapping.

Basics of subwavelength field mapping

Near fields (Box 1) are intrinsically hard to image directly, as they cannot be viewed by, for example, a CCD array or photodiode. This is because near fields are evanescent in nature and hence, for visible or near-infrared light, these fields are typically found within 10s or 100s of nanometres of a surface. Consequently, an intermediate step is required, whereby some of the near field is converted to far field. This conversion may be achieved in several ways. For example, information about the nanoscopic fields may be accessed by incorporating emitters such as dye molecules into a nanophotonic structure and studying the resultant fluorescence[12], or by using photoresist which polymerizes at high intensities and hence creates a permanent record of subwavelength regions of high field intensities[13]. Such methods, however, are rather specialized as they permanently alter structures or only access a select few properties of the light fields such as their intensities.

In fact, an ideal method would map out nanoscale light fields without perturbing either the physical structure under investigation or its near field. Further, such a technique should be flexible, allowing for the study of a variety of different structures and providing the maximal amount of information about their nanoscopic fields. Clearly, such an optimal, one-way interaction is impossible, as the act of bringing some of the near field into the far field must in some way change the system. However, modern near-field scanning optical microscopes (NSOMs) can come very close to the ideal scenario outlined above. While a comprehensive review of the operation of NSOMs[14–21] or their historical development[22] is beyond our current scope, we will focus on the recently emerged aspects of this technique that strive towards a complete mapping of the near field.

The essence of near-field optical microscopy, as sketched in Fig. 1, is very simple. A nanoscopic object, the near-field probe, is brought into the near field, where it scatters some of the light into the far field. There are two main approaches to this type of near-field mapping, each with its own strengths, which roughly depend on the type of probe that is used. In aperture probe (AP) near-field microscopy, the light that is converted to far-field radiation is collected (c-NSOM) through the probe (Fig. 1a), while a scattering NSOM (s-NSOM) uses an apertureless tip to scatter some light to free space (Fig. 1b), where it can be detected by, for example, a photodiode. In either case, the tip is brought to within a height of 10s of nanometres above the structure, and then raster-scanned to map the near-field distribution. Care must be taken that the interaction between the near-field tip and the sample is understood[17,23]. Clearly, in order to obtain an optical signal, the near-field probe has to frustrate the evanescent field, so interaction is required. Nevertheless, the tip–sample interaction should, in general, be so weak that the measured near fields represent the fields without the presence of the probe. In other words, the interaction should be in the regime of first-order perturbation. The excellent agreement of many of the measurements presented below with theoretical calculations shows that this is usually the case. In certain situations, however, the interaction of the probe with the sample cannot be neglected, and first-order perturbation theory is no longer sufficient to model the measurements. In such situations the presence of the probe can, for example, change the near-field distributions or even their spectral contents. Higher-order terms, where for example light scatters from the sample to the probe and back, need to be taken into account. They can be modelled allowing for the reconstruction of the near-field distributions even

FOM Institute AMOLF, Science Park 104, 1098 XG Amsterdam, The Netherlands. *e-mail: kuipers@amolf.nl

NATURE PHOTONICS DOI: 10.1038/NPHOTON.2010.285

Box 1 | Near fields.

Any monochromatic light field can, for a moment in time, be written as

$$\mathbf{E}(\mathbf{r}) = \begin{pmatrix} A_1(\mathbf{r})\, e^{i\varphi_1(\mathbf{r})} \\ A_2(\mathbf{r})\, e^{i\varphi_2(\mathbf{r})} \\ A_3(\mathbf{r})\, e^{i\varphi_3(\mathbf{r})} \end{pmatrix} \quad (1)$$

where $A_m(\mathbf{r})$ and $\phi_m(\mathbf{r})$ are the spatially dependent amplitude and phase distributions of the three vector components of the field (for example, $m = 1,2,3 = x,y,z$ in Cartesian coordinates). This field can be decomposed into a set of waves according to

$$\mathbf{E}(\mathbf{r}) = \int_{-\infty}^{\infty} \tilde{\mathbf{E}}_{\mathbf{k}} e^{i\mathbf{k}\cdot\mathbf{r}} d\mathbf{k} \quad (2)$$

where $\mathbf{r}$ denotes a spatial position, and each wave in the decomposition is indexed by its wavevector $\mathbf{k}$ and a complex amplitude $\tilde{\mathbf{E}}_{\mathbf{k}}$. A similar expression can be written for the corresponding magnetic field $\mathbf{H}$. For a far-field distribution in a non-absorbing medium (index of refraction n is real) $\mathbf{k}$ is real and its amplitude is $k_0 = \sqrt{(k_x^2 + k_y^2 + k_z^2)} = 2\pi n/\lambda$, for a vacuum wavelength λ. Hence a far-field light distribution can always be described in terms of a superposition of plane waves. If, however, $k_x^2 + k_y^2 > k_0^2$ as is the case for a bound mode, then k_z must have an imaginary component. As can be seen from Eq. (2), the imaginary k_z results in an exponentially decaying wave. Such waves are said to be evanescent, and, as is sketched in Fig. B1, they dominate in the near field of their source. That is, unlike far fields which propagate through space, near fields are typically localized to an emitter or interface. Further, because the real part of near-field wavevectors is larger than k_0, structure can be found in near fields that is well below the diffraction limit of far fields, allowing them to be used for super-resolution imaging[21,97].

At the nanoscale, near fields can be tailored through the geometry of the structures about which they are found. Consequently, researchers can design structures such as nanoantennas that focus and direct light fields on the nanoscale[98], or create waveguides that allow for light propagation at subwavelength dimensions[99] with, for example, variable velocities[100]. The near fields of such structures can have complex structure and, in contrast to typical far fields, often have non-zero amplitude in all six field components. This complete electromagnetic presence is exemplified in the inset of Fig. B1, which shows the calculated[101] near fields 200 nm above a W1 silicon membrane photonic crystal waveguide. Here, not only are all components present, but they also have distinctly different amplitude, $A(\mathbf{r})$, and phase, $\phi(\mathbf{r})$ (not shown), distributions. Interestingly, since near fields such as those shown in this figure are made of waves with different wavevectors, each with a different k_z, they can have vastly different distributions at different heights above their sources[3].

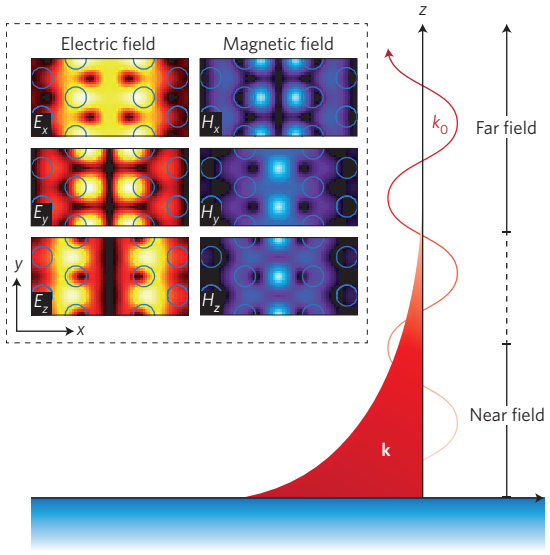

Figure B1 | Optical near-fields. Schematic of the near- and far-field regions of an interface. The evanescent near field typically dominates for about a wavelength, after which its contribution quickly becomes negligible and only propagating far fields remain. The inset shows the calculated electric and magnetic near-field amplitude distributions 200 nm above a W1 silicon photonic crystal waveguide for $\lambda = 1{,}570$ nm. The light propagates in y, and z points out of the plane. The solid lines outline the holes of the photonic crystal, which have a radius of 120 nm.

in this regime of strong probe–sample interaction[24]. In fact, as we show below, such strong interactions can even be beneficial if they are properly understood. For example, a near-field probe can be used to tune optical modes of nanoantennas[23] or nanocavities[25,26], and, by monitoring the spectral response of these structures, additional information about the nanoscale optical properties of these structures can be revealed.

Because the conversion of near fields to far-field radiation is mediated by the probe tip, the quality[27] and properties of NSOM mappings are crucially dependent on this tip. Hence, near-field tips must be made in a reproducible manner that allows for control over their parameters, for example using focused ion beam milling[28] or etching techniques[29]. Scattering NSOM tips, such as those shown in the inset to Fig. 1b, are ultrasharp, allowing sub-10-nm resolution[30,31], and even single-molecule detection[32]. Further, s-NSOM tips can be made resonant with light ranging from the visible[33] to the infrared[34], and even in the terahertz (THz) region[35]. Clearly, new physics becomes accessible whenever a new region of the spectrum is opened up. For example, opening up the infrared and THz regimes has allowed near-field studies of graphene plasmonics[36,37]. In AP near-field microscopy, in collection mode (Fig. 1a), the near field is collected through the probe, which is generally a two-layered system consisting of a tapered waveguide and a metallic coating. There are several variants on the standard AP, which has a circular aperture with a typically diameter ranging from 100 to 250 nm as shown in the inset of Fig. 1a. Special probes, such as those based on extraordinary optical transmission[38] or the 'campanile' probe[39], are designed to increase the throughput, detect specific components of the near field, or improve the resolution of the NSOM. A few probes, such as the split-ring probe (SRP)[40], bowtie probe[41] or pyramid probe[42] that will be covered below, are designed to access near-field information that is often unavailable with standard APs. In all cases, unlocking the full potential of these probes requires a deep understanding of the way in which they interact with light at the nanoscale. As this understanding grows together with improved nanofabrication of the probes, so too does our ability

to access different aspects of the near field. Even for the simple AP, such an understanding is far from complete, and unexpected capabilities may yet be discovered.

There are several ways to try to understand the way in which a probe converts light from near-field to far-field radiation. Traditionally, the near field is assumed to induce dipoles at the tip of the NSOM probe, which then radiate into the far field, as is sketched out in Fig. 1. For s-NSOM, induced dipoles are usually taken to be one out-of-plane and one in-plane electric dipole, where the probed in-plane dipole orientation is determined by the location of the detector[43]. Likewise, it has long been accepted that for the standard AP used in collection mode NSOM, the dominant dipoles are the two in-plane electric dipoles. Recent work, however, has shown that nanoscopic structures such as subwavelength holes in metallic films[44] or semiconductor nanoparticles[45] respond to both the electric and magnetic fields. As we show below, this total electromagnetic response of the objects at the nanoscale also applies to the probe tip, and hence near-field microscopy need not be limited to the detection of electric fields. This suggests that the simple picture of the probe tip as a couple of electric dipoles may not always be sufficient to understand, or model, its operation: other multipoles, including magnetic dipoles, might be needed. In fact, a different framework based on reciprocity has recently been introduced to explain the near- to far-field conversion of radiation by an NSOM probe[46]. Using reciprocity, the structured near fields detected by the probe can be related to the fields that a simple dipole would transmit through the probe, fields that are readily calculable. This approach has been successfully applied to both scattering[47] and aperture[48] NSOMs.

Visualizing electric fields

Recent advances to near-field microscopy have allowed us to map more than just the intensity of the near field. Now, when we peer into the near field, we measure both phase $\phi(\mathbf{r})$ and amplitude $A(\mathbf{r})$, usually by using an interferometric scheme[49–51], as sketched in Fig. 2. Such phase information can be used in conjunction with the resolution of an s-NSOM to, for example, study the fundamental nature of the resonances that control light–matter interactions in structures such as split-ring resonators[52], nanoantennas[5,6] (Fig. 2d) and metamolecules[53,54]. Similarly, phase-sensitive c-NSOM measurements have allowed studies of mode properties of light as it propagates through nanoscopic waveguides, such as plasmonic nanowires[55] (Fig. 2c), and as it interacts with negative-index metamaterials[56]. Importantly, high-resolution phase-sensitive measurements can be Fourier transformed, allowing the near field to be visualized in momentum space (k-space). As a first demonstration of this technique, researchers studied the details of the Bloch harmonics that form a propagating mode of a photonic crystal waveguide[57]. Subsequently, imaging and filtering in k-space allows studies of dielectric-clad waveguides[58], and the separation of forward and backward propagating (or TE and TM) waves, essentially correcting for unwanted reflections or imperfect incoupling in experiments[59].

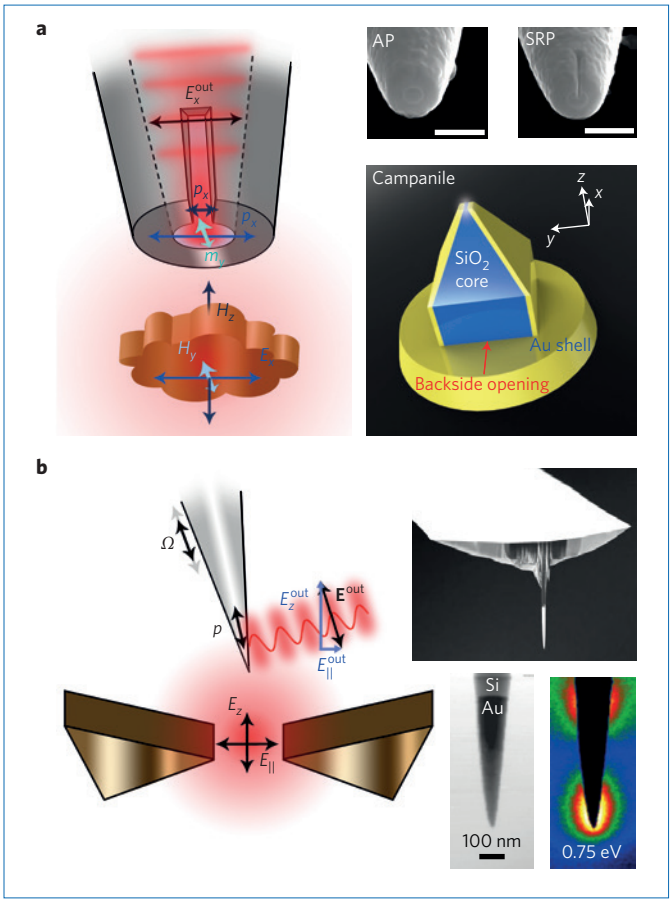

Figure 1 | Near-field scanning optical microscopy. a,**b**, An aperture (**a**) and scattering (**b**) nanoscopic probe is brought into the near field of a structure. The interaction of the tip of the probe with the light converts a very small amount of near-field to far-field radiation, where it can be detected by standard free-space optics. In both sketches the dominant dipoles, which mediate the near- to far-field radiation, are shown. In **a**, the detection channel x-oriented light is shown as an example. For a standard aperture probe (top left inset), the detected field E_x^{out} arises from both E_x and H_y of the sample, while a split-ring probe (top right inset) will also measure H_z owing to charge build-up across the slit[40]. Likewise, the detected E_y^{out} (not shown) will be composed of E_y and H_x. The bottom inset shows a sketch of a campanile probe, which acts like an aperture probe, but with a greatly enhanced sensitivity to the near field that is oriented parallel to the gap at its tip (adapted from ref. 39). Panel **b** shows that, for a scattering NSOM, the detected field is composed of both an in-plane component $E_{||}$ and an out-of-plane component E_z, where their ratio and the orientation of $E_{||}$ are set by the direction at which $\mathbf{E}^{out}$ is detected. The inset in **b** shows a typical scattering probe tip on a cantilever with a zoom-in on the probe tip (bottom left inset), which in this case is resonant in the infrared (from ref. 96).

Mapping electric vector fields. Light fields are vector quantities, meaning that the orientation of the fields is just as important as their amplitude. In total there are six possible electromagnetic components — three electric and three magnetic — and fully understanding light–matter interactions at the nanoscale typically requires knowledge of all six (Box 1). As early as the 1990s, single molecules were used as probes to determine the orientation of near fields[32,60,61], in much the same way as a well-characterized nanoparticle was recently used to map out vector light-field distributions[62]. Polarization-sensitive NSOM, however, was first demonstrated in 2002, where illumination through an aperture probe allowed the combinations of the vector components of the local optical density of states to be mapped for a nanophotonic structure[63]. It was not until 2007, however, that a clever use of free-space polarization optics allowed researchers to first map out different components of the near field. In this first experiment an s-NSOM was used, and hence the amplitudes of the E_z and $E_{||} = E_x$ components of the near field were mapped, where the choice of the in-plane component was determined by the positioning of the detector relative to the sample and tip[64]. Shortly after, this technique was applied to interferometric c-NSOM and then s-NSOM measurements to separately map the complex E_x and E_y (c-NSOM, ref. 59), and E_z and E_x (s-NSOM, ref. 65). Using c-NSOM operating in this mode has made it possible to study features such as polarization singularities carrying spin angular momentum in the near fields of

NATURE PHOTONICS DOI: 10.1038/NPHOTON.2010.285

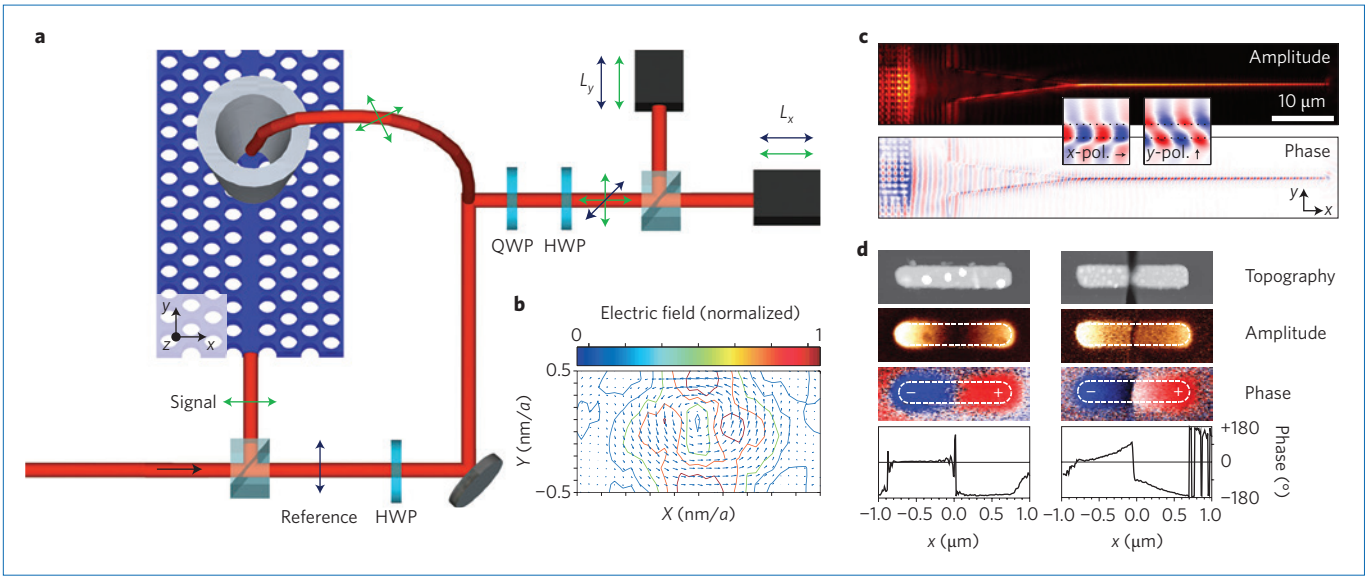

Figure 2 | Vector light field mappings with NSOMs. a, Schematic of a phase- and polarization-sensitive NSOM measurement (adapted from ref. 48). Laser light is split into a signal and a reference branch, which are interfered to provide the phase information. Careful polarization control with the waveplates allows for the separation of the different components of the in-plane fields, as denoted by the arrows. HWP, half-wave plate; QWP, quarter-wave plate. **b**, Example of the instantaneous vector electric field magnitude measured above a unit cell of size *a*, as shown on the axes, of a photonic crystal waveguide, as is sketched in **a** (adapted from ref. 59). **c**, Vector near-field measurements shed light on the adiabatic mode transformation of planar plasmons to nanowire plasmons. In the amplitude (top) and real part of the field maps (bottom) both the hole array that excites the plasmons and the taper that leads to the nanowire are visible. The insets show different components of the plasmon fields (adapted from ref. 55). **d**, Vector infrared s-NSOM measurements demonstrate how loading nanoantennas (1,550 nm long) by cutting a continuous rod antenna (left) so that the two halves are only connected by a small metal bridge (right) can shape and control their near field (adapted from ref. 5).

photonic crystal waveguides[59] (Fig. 2b), and more recently has been crucial to unravelling the optical response of nanoscopic plasmonic scatterers such as subwavelength holes[66]. Concurrently, vector near-field mappings with s-NSOMs have shed light on the way in which nanoantennas confine light[65], and on the coupling of plasmonic nanowire arrays[67].

Beyond the vector nature. There are other important aspects of structured, nanoscopic light fields, beyond their vector nature, which can be addressed by near-field microscopy. One such aspect is that near fields, and indeed the optical response of the structures that support them, can display dynamics, often on picosecond or femtosecond timescales. To access ultrafast phenomena at the nanoscale, a femtosecond laser source was integrated into an interferometric NSOM, initially tracking the spatiotemporal evolution of ultrashort pulses propagating in ridge waveguides[68]. Subsequently, this technique allowed studies to be made of slow light propagation, both in dielectric photonic crystal waveguides[4] and in plasmonic waveguides[69], and even of single plasmonic scattering events where a temporal resolution below 50 fs was required[44].

There are two principal modes of operation for a time-resolved NSOM. First, high-resolution spatial maps can be taken at different time steps, like a series of frames in a movie[4,68]. In fact, if the complex vector fields are known with sufficient spatial resolution then a Fourier transform of the frames will yield the *k*-space dynamics of the system, as is shown in Fig. 3a. Such a study can show how the different eigenmodes of complex photonic structures couple to each other even when they are co-located in space, demonstrating, for example, directional coupling[70].

The second mode of operation of a time-resolved NSOM is when high-resolution temporal scans are taken at different positions. Essentially, the NSOM probe is positioned at a certain location, and the time delay between the signal and reference branches is scanned, measuring the cross-correlation between a known reference pulse and the local temporal dynamics of the local near field. In the previous examples, the peak in these line traces was often used to track the time at which a pulse passed a certain point in the structure[69]. Much more information can be gained, however, if the complex field is known at every point in time with sufficient resolution. In this case, the time trace of the field can be Fourier transformed to provide the spectral density of the near field at that location, for example allowing studies of the vibrational dynamics of polymers with nanoscale resolution[71].

The spectral content of near fields is, in fact, another important quantity that can be measured, and that provides additional information on light–matter interactions at the nanoscale. As mentioned above, this information can be gained through Fourier transform spectroscopy and, when coupled to an NSOM with a broadband light source, it opens up many new avenues of research. Using this technique with a broadband thermal source allows, for example, nanoscale mappings of dopant concentrations in semiconductors[72] (Fig. 3b) and studies of the thermal near fields[73]. Likewise, by integrating a broadband laser into the NSOM, the near-field distributions of protein complexes[74] (Fig. 3c) or even the crystal structure of nanoscale domains in an organic film[75] (Fig. 3d), can be mapped. NSOM is therefore ideally suited for spectroscopy of anisotropic samples with nanoscale resolution. The near-field spectrum distribution can also be directly mapped by spectrally analysing the light collected by a c-NSOM probe. Although this is not an interferometric technique, and hence does not result in phase-sensitive near-field mappings or signal amplification, it can be used as a point-to-point probe of light propagating in complex photonic elements[76], or integrated photonic chips[77]. In particular, and unlike interferometric approaches, here new frequencies that are created during pulse propagation can still be detected, making this method particularly suitable for nonlinear optics experiments[77].

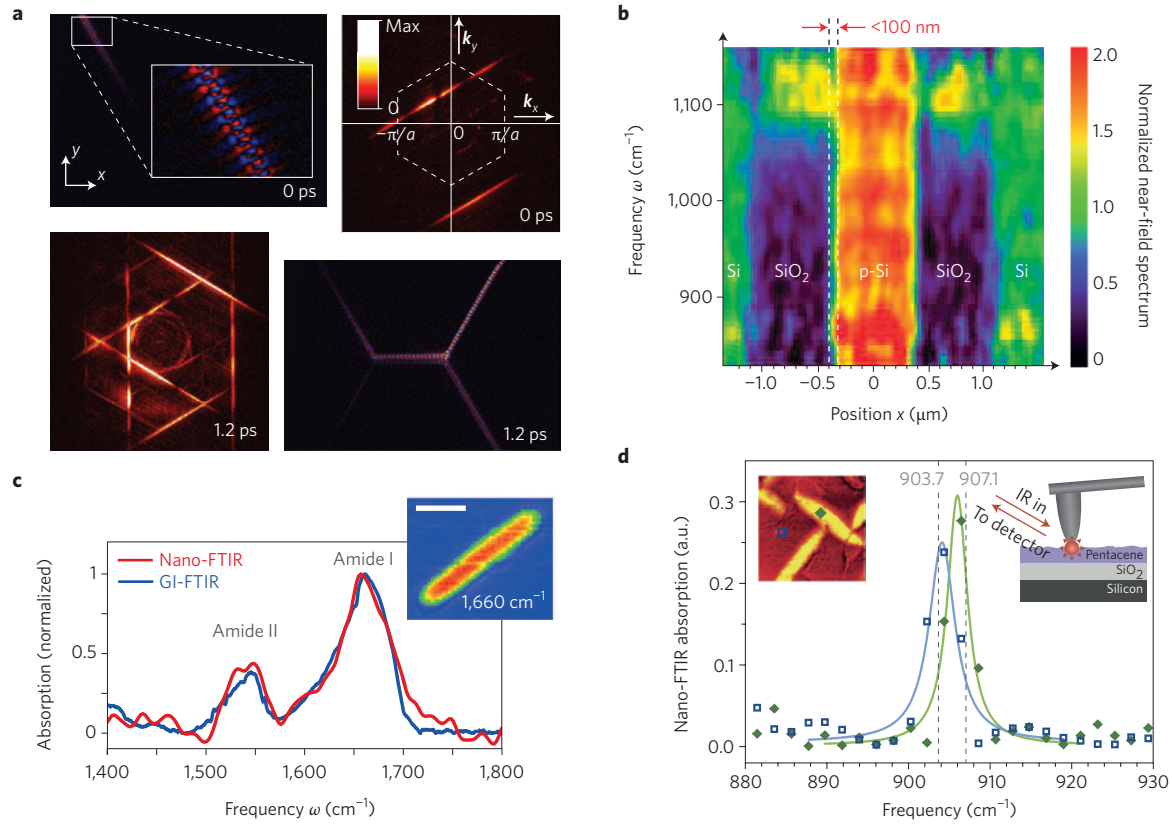

Figure 3 | Examples of time- and frequency-resolved near-field mappings. a, Real- and *k*-space mappings of a pulse propagating through a photonic crystal directional coupler. At 0 ps (top row) the pulse enters the coupler, while at 1.2 ps (bottom row) it has travelled through most of the structure and is seen exiting through both output ports. In *k*-space, additional eigenmodes of the structure are populated (light up) as the pulse propagates through the coupler (adapted from ref. 70). **b**, Infrared near-field spectra of a five-layer (silicon/silicon oxide/p-doped silicon/silicon oxide/silicon) structure taken with Fourier transform infrared (FTIR) spectroscopy with a thermal light source. The different layers display markedly different optical responses, allowing subdiffraction mappings of the doping levels (adapted from ref. 72). **c**, FTIR spectra of the near field of a single tobacco mosaic virus (red curve), taken with a broadband laser source, compared with far-field spectra from arrays of the virus (blue curve). Both spectra show two resonances associated with vibrational modes of the virus. GI, grazing incidence. The inset shows the near-field phase-contrast map taken at the peak of the resonance, with a scale bar corresponding to 100 nm (adapted from ref. 74). **d**, NSOM FTIR spectra of two positions of a thin pentacene film, allowing discrimination between the thin film (blue) and bulk phases (green). The spectra can be taken with 20-nm spatial resolution. a.u., arbitrary units. The insets show (right) a schematic of the experiment and (left) spatial map of the FTIR spectra taken at a single frequency 907.1 cm^{-1} (reproduced from ref. 75).

Mapping the full electromagnetic near field

While there has been tremendous recent progress towards a full map of electric near fields, such maps only tell half the story of light–matter interactions at the nanoscale; the other half is told by magnetic field mappings. With the advent of magnetically active structures, such as metamaterials[78], knowledge gained from the mappings of **H**, in addition to **E**, is increasingly crucial. It is tempting to invoke Maxwell's equations, which relate these quantities. But in order to derive **H** from **E**, all three components of the electric field need to be known with sufficient precision and spatial accuracy, in a three-dimensional space, to allow for accurate differentiation. As we discussed above, such complete mappings of **E** are technically challenging and, to date, have not been demonstrated. Consequently, knowledge of the magnetic near-field distributions demands direct, near-field measurements.

Sensitivity to magnetic near fields. A mapping of optical magnetic fields at the nanoscale was first demonstrated using a c-NSOM with a slit etched into the probe tip[40] (Fig. 1a). This etching effectively turned the probe aperture into a split-ring resonator that, in essence, could convert the out-of-plane component of the magnetic field (H_z) into measurable in-plane far-field radiation (E_x or E_y, depending on the slit orientation). Recently, a new c-NSOM probe type was introduced, the pyramid probe[42], that was engineered to collect one of the in-plane magnetic fields (H_x or H_y, depending on the aperture orientation) much more efficiently than the in-plane electric fields that would normally be detected by an aperture probe. Such a probe has enabled studies of the magnetic response of plasmonic nanoantennas[79] (Fig. 4a). With the addition of the split-ring and pyramid probes, all six components of the near field have become accessible to NSOMs, albeit not in a single measurement, or even with a single type of NSOM. Special probes, however, are not easy to fabricate or align and use in an NSOM. In particular, for a case such as the split-ring probe, where three signals are simultaneously measured (E_x, E_y and H_z) using only two detectors, disentangling these fields requires additional constraints such as symmetries in the near fields (and hence in the structures)[80].

Concurrently with the development of the specialized probes, researchers discovered that typical aperture probes, such as the one shown in Fig. 1a, are also sensitive to magnetic near fields. Initially, it was shown that through an interaction mediated by H_z, an aperture probe could be used to control photonic crystal nanocavity

NATURE PHOTONICS DOI: 10.1038/NPHOTON.2010.285

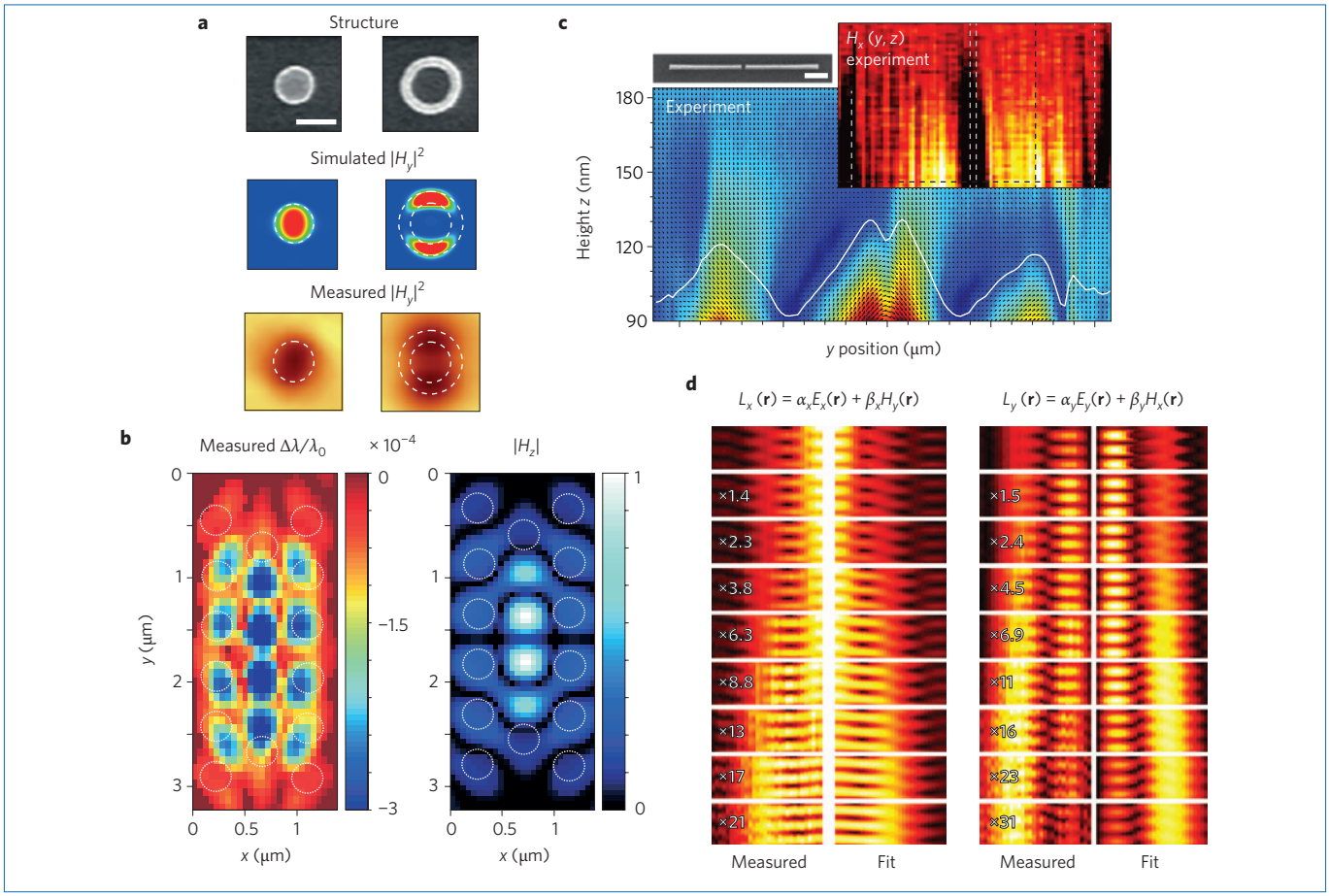

Figure 4 | Electromagnetic near-field maps. a, An example of magnetic near-field maps (in this case, of H_y) of single nanostructures taken with a pyramid-probe c-NSOM (adapted from ref. 79). **b**, Measurements of the resonance shift of a photonic crystal nanocavity, normalized to the unshifted cavity resonance at λ_0 = 1534.6 nm, taken with a regular aperture-probe c-NSOM. From these measurements, the distribution of H_z of the unperturbed cavity can be inferred (adapted from ref. 81). **c**, s-NSOM measurements on a symmetry plane of a nanoantenna (top left inset, scale bar represents 500 nm), allowing the full mapping of E_y, E_z and H_x on the plane (adapted from ref. 87). **d**, c-NSOM near-field maps, and fits, at different heights (from 20 to 400 nm) above a photonic crystal waveguide (see Fig. 2a) containing information of all four components of the in-plane electromagnetic fields (adapted from ref. 48).

resonances[81,82]. In fact, this interaction can be used to map H_z of cavities without the need for a specialized probe (Fig. 4b), and also to study localization of electromagnetic energy in disordered structures[83,84]. Researchers then realized that an aperture probe is very similar to a Bethe-hole analyser, which should mainly be sensitive to the in-plane magnetic fields. Hence, by choosing a correct aperture size and metal coating thickness, NSOM mappings were made of H_x and H_y (along with E_z from the scattered light) of a plane wave[85,86].

Simultaneous measurements of E and H. In 2010, Olmon *et al.*[87] showed that high-resolution s-NSOM measurements on a symmetry plane of a nanoantenna could be used to determine the complete electromagnetic near field. This type of complete mapping, which is shown in Fig. 4c, is only possible on the symmetry plane, where certain field components are identically zero. On this plane, knowledge of two non-zero (E_y and E_z) components is sufficient for Maxwell's equations to yield the remaining component (H_x). As with the recent measurements with a split-ring aperture probe[80], exploiting the symmetries of the near fields allowed for mapping of three field components, two electric and one magnetic. Similarly, instead of symmetry, numerical simulations can be used in addition to partial near-field measurements to determine the full vectorial light field. This concept was nicely demonstrated in 2010, where measurements of the in-plane electric field with a dielectric probe were used as a boundary condition for finite-difference time-domain calculations to reconstruct all of the magnetic field components[88].

The demonstration that a normal aperture probe could be sensitive to the in-plane magnetic fields[85] suggested that a more complete mapping of the near field should be possible. In fact, it has now been established[48] that, in the near field, an aperture probe is sensitive to the in-plane components of both **E** and **H**, and not just one, as had been previously assumed. Measurements of the near field of a photonic crystal waveguide, taken at different heights above its surface (Fig. 4d), show that typical aperture probes are roughly equally sensitive to electric and magnetic fields, in good agreement with reciprocal-based modelling[46,48]. That is, a c-NSOM collects light from four components, E_x, E_y, H_x and H_y, at the same time, allowing mappings of nanophotonic structures that are electrically and magnetically active.

Outlook

We can now routinely access a variety of properties of the electromagnetic near field and create mappings well beyond the original electric field amplitude images. Further, NSOMs now operate at the extreme conditions required to study some samples, such as at cryogenic temperatures and at high magnetic fields[89]. There

are, however, many challenges ahead as we progress towards the complete mapping of electromagnetic near fields. Currently, at most four of the six components of the near field, namely the in-plane electric and magnetic field components, have been simultaneously detected. These four field components are, however, contained within two signals, and unravelling the individual components is far from trivial. Such an unravelling has only been shown for structures, such as the photonic crystal waveguide, where the separate field components are known *a priori*. A more general separation approach remains a work in progress. Likewise, a simultaneous full measurement of all six components remains a challenge for the future. Such a measurement could perhaps involve a split-ring probe NSOM with signals collected both through the aperture and from the scattered light, or a combination of high-resolution three-dimensional mapping of some of the near-field components in conjunction with electromagnetic theory.

Although the ability to map the near field will undoubtedly grow, near-field optical microscopy is already an extremely powerful tool. Capabilities such as high-resolution, Fourier transform infrared s-NSOM allow studies of correlated systems such as high-temperature superconductors or topological insulators[90] and organic systems[74,75]. Quantum nanophotonics is another emerging field that stands to gain from NSOM measurements that, for example, can be used to map the local density of optical states near a nanoscale structure, a quantity that is intrinsically linked to the emission from quantum emitters[63]. In fact, the emission from a dipole source into the modes of a nanophotonic structure, which depends intimately on the vector distribution of the near field, can even be mapped using polarization-resolved NSOM in illumination mode, an important step towards solid-state quantum architecture[91–93]. Further, accessing the magnetic, in addition to the electric, near fields with c-NSOMs allows for studies of magnetically active structures such as split-ring resonators or magnetic molecules, and even studies of the way in which nanostructured metasurfaces can control the flow of light[94,95]. Finally, nonlinear and spectral properties, as well as temporal dynamics of light–matter interactions, at the nanoscale can already be directly visualized with the techniques outlined in this Review, ensuring that near-field optics remains an integral part of the understanding and development of the field of nanophotonics.

Received 7 July 2014; accepted 20 October 2014; published online 27 November 2014

References

1. Gay, G. *et al.* The optical response of nanostructured surfaces and the composite diffracted evanescent wave model. *Nature Phys.* **2,** 262–267 (2006).
2. Lalanne, P. & Hugonin, J. P. Interaction between optical nano-objects at metallo-dielectric interfaces. *Nature Phys.* **2,** 551–556 (2006).
3. Bozhevolnyi, S. I. *et al.* Near-field imaging of light propagation in photonic crystal waveguides: Explicit role of Bloch harmonics. *Phys. Rev. B* **66,** 235204 (2002).
4. Gersen, H. *et al.* Real-space observation of ultraslow light in photonic crystal waveguides. *Phys. Rev. Lett.* **94,** 073903 (2005).
5. Schnell, M. *et al.* Controlling the near-field oscillations of loaded plasmonic nanoantennas. *Nature Photon.* **3,** 287–291 (2009).
6. Dorfmüller, J. *et al.* Near-field dynamics of optical Yagi-Uda nanoantennas. *Nano Lett.* **11,** 2819–2824 (2011).
7. Kauranen, M. & Zayats, A. V. Nonlinear plasmonics. *Nature Photon.* **6,** 737–748 (2012).
8. Li, J. F. *et al.* Shell-isolated nanoparticle-enhanced Raman spectroscopy. *Nature* **464,** 392–395 (2010).
9. López-Tejeira, F. *et al.* Efficient unidirectional nanoslit couplers for surface plasmons. *Nature Phys.* **3,** 324–328 (2007).
10. Minovich, A. *et al.* Generation and near-field imaging of Airy surface plasmons. *Phys. Rev. Lett.* **107,** 116802 (2011).
11. Juan, M. L., Righini, M. & Quidant, R. Plasmon nano-optical tweezers. *Nature Photon.* **5,** 349–356 (2011).
12. Yoon, I. *et al.* Profiling the evanescent field of nanofiber waveguides using self-assembled polymer coatings. *Nanoscale* **5,** 552–555 (2013).
13. Sundaramurthy, A. *et al.* Toward nanometer-scale optical photolithography: utilizing the near-field of bowtie optical nanoantennas. *Nano Lett.* **6,** 355–360 (2006).
14. Paesler, M. A. & Moyer, P. J. *Near-field Optics: Theory, Instrumentation, and Applications* (Wiley, 1996).
15. Hecht, B. *et al.* Scanning near-field optical microscopy with aperture probes: Fundamentals and applications. *J. Chem. Phys.* **112,** 7761–7774 (2000).
16. Dereux, A., Girard, C. & Weeber, J.-C. Theoretical principles of near-field optical microscopies and spectroscopies. *J. Chem. Phys.* **112,** 7775–7789 (2000).
17. Kawata, S., Ohtsu, M. & Irie, M. *Nano-optics* (Springer, 2002).
18. Courjon, D. *Near-field Microscopy and Near-field Optics* (World Scientific, 2003).
19. Zayats, A. V. & Richards, D. *Nano-optics and Near-field Optical Microscopy* (Artech House, 2008).
20. Vogelgesang, R. & Dmitriev, A. Real-space imaging of nanoplasmonic resonances. *Analyst* **135,** 1175–1181 (2010).
21. Novotny, L. & Hecht, B. *Principles of Nano-optics* (Cambridge Univ. Press, 2012).
22. Novotny, L. in *Progress in Optics* Vol. 50 (ed. Wolf, E) Ch. 5, 137–184 (Elsevier, 2007).
23. García-Etxarri, A., Romero, I., de Abajo, F. J. G., Hillenbrand, R. & Aizpurua, J. Influence of the tip in near-field imaging of nanoparticle plasmonic modes: Weak and strong coupling regimes. *Phys. Rev. B* **79,** 125439 (2009).
24. Sun, J., Carney, P. S. & Schotland, J. C. Strong tip effects in near-field scanning optical tomography. *J. Appl. Phys.* **102,** 103103 (2007).
25. Koenderink, A. F., Kafesaki, M., Buchler, B. C. & Sandoghdar, V. Controlling the resonance of a photonic crystal microcavity by a near-field probe. *Phys. Rev. Lett.* **95,** 153904 (2005).
26. Lalouat, L. *et al.* Near-field interactions between a subwavelength tip and a small-volume photonic-crystal nanocavity. *Phys. Rev. B* **76,** 041102(R) (2007).
27. Hecht, B., Bielefeldt, H., Inouye, Y., Pohl, D. W. & Novotny, L. Facts and artifacts in near-field optical microscopy. *J. Appl. Phys.* **81,** 2492–2498 (1997).
28. Veerman, J. A., Otter, A. M., Kuipers, L. & van Hulst, N. F. High definition aperture probes for near-field optical microscopy fabricated by focused ion beam milling. *Appl. Phys. Lett.* **72,** 3115–3117 (1998).
29. Stökle, R. *et al.* High-quality near-field optical probes by tube etching. *Appl. Phys. Lett.* **75,** 160–162 (1999).
30. Bek, A., Vogelgesang, R. & Kern, K. Apertureless scanning near field optical microscope with sub-10 nm resolution. *Rev. Sci. Instrum.* **77,** 043703 (2006).
31. Fleischer, M. *et al.* Gold nanocone near-field scanning optical microscopy probes. *ACS Nano* **5,** 2570–2579 (2011).
32. Betzig, E. & Chichester, R. J. Single molecules observed by near-field scanning optical microscopy. *Science* **262,** 1422–1425 (1993).
33. Wang, L. & Xu, X. High transmission nanoscale bowtie-shaped aperture probe for near-field optical imaging. *Appl. Phys. Lett.* **90,** 261105 (2007).
34. Jones, A. C. *et al.* Mid-IR plasmonics: near-field imaging of coherent plasmon modes of silver nanowires. *Nano Lett.* **9,** 2553–2558 (2009).
35. Huber, A. J., Keilmann, F., Wittborn, J., Aizpurua, J. & Hillenbrand, R. Terahertz near-field nanoscopy of mobile carriers in single semiconductor nanodevices. *Nano Lett.* **8,** 3766–3770 (2008).
36. Chen, J. *et al.* Optical nano-imaging of gate-tunable graphene plasmons. *Nature* **487,** 77–81 (2012).
37. Fei, Z. *et al.* Gate-tuning of graphene plasmons revealed by infrared nano-imaging. *Nature* **487,** 82–85 (2012).
38. Neumann, L. *et al.* Extraordinary optical transmission brightens near-field fiber probe. *Nano Lett.* **11,** 355–360 (2011).
39. Bao, W. *et al.* Mapping local charge recombination heterogeneity by multidimensional nanospectroscopic imaging. *Science* **338,** 1317–1321 (2012).
40. Burresi, M. *et al.* Probing the magnetic field of light at optical frequencies. *Science* **326,** 550–553 (2009).
41. Vo, T.-P. *et al.* Near-field probing of slow Bloch modes on photonic crystals with a nanoantenna. *Opt. Express* **20,** 4124–4135 (2012).
42. Denkova, D. *et al.* Mapping magnetic near-field distributions of plasmonic nanoantennas. *ACS Nano* **7,** 3168–3176 (2013).
43. Koglin, J., Fischer, U. C. & Fuchs, H. Material contrast in scanning near-field optical microscopy at1–10 nm resolution. *Phys. Rev. B* **55,** 7977 (1997).
44. Rotenberg, N. *et al.* Plasmon scattering from single subwavelength holes. *Phys. Rev. Lett.* **108,** 127402 (2012).
45. Du, Y. H., Kuznetsov, A. I., Miroshnichenko, A. E., Yu, Y. F. & Luk'yanchuk, B. Directional visible light scattering by silicon nanoparticles. *Nature Commun.* **4,** 1527 (2012).
46. Porto, J. A., Carminati, R. C. & Greffet, J-J. Theory of electromagnetic field imaging and spectroscopy in scanning near-field optical microscopy. *J. Appl. Phys.* **88,** 4845–4850 (2000).

47. Esslinger, M. & Vogelgesang, R. Reciprocity theory of apertureless scanning near-field optical microscopy with point-dipole probes. *ACS Nano* **6,** 8173–8182 (2012).
48. le Feber, B., Rotenberg, N., Beggs, D. M. & Kuipers, L. Simultaneous measurement of nanoscale electric and magnetic optical fields. *Nature Photon.* **8,** 43–46 (2014).
49. M. L. M. Balistreri, L. K., J. P. Korterik & van Hulst, N. F. Local observations of phase singularities in optical fields in waveguide structures. *Phys. Rev. Lett.* **85,** 294–297 (2000).
50. Nesci, A., Dändliker, R. & Herzig, H. P. Quantitative amplitude and phase measurement by use of a heterodyne scanning near-field optical microscope. *Opt. Lett.* **26,** 208–210 (2001).
51. Ocelic, N., Huber, A. & Hillenbrand, R. Pseudoheterodyne detection for background-free near-field spectroscopy. *Appl. Phys. Lett.* **89,** 101124 (2006).
52. Zentgraf, T. *et al.* Amplitude- and phase-resolved optical near fields of split-ring-resonator-based metamaterials. *Opt. Lett.* **33,** 848–850 (2008).
53. Deutsch, B., Hillenbrand, R. & Novotny, L. Visualizing the optical interaction tensor of a gold nanoparticle pair. *Nano Lett.* **10,** 652–656 (2010).
54. Alonso-Gonzalez, P. *et al.* Real-space mapping of Fano interference in plasmonic metamolecules. *Nano Lett.* **11,** 3922–3926 (2011).
55. Verhagen, E., Spasenović, M., Polman, A. & Kuipers, L. Nanowire plasmon excitation by adiabatic mode transformation. *Phys. Rev. Lett.* **102,** 203904 (2009).
56. Burresi, M. *et al.* Negative-index metamaterials: looking into the unit cell. *Nano Lett.* **10,** 2480–2483 (2010).
57. Gersen, H. *et al.* Direct observation of Bloch harmonics and negative phase velocity in photonic crystal waveguides. *Phys. Rev. Lett.* **94,** 123901 (2005).
58. Ayache, M., Nezhad, M. P., Zamek, S., Abashin, M. & Fainman, Y. Near-field measurement of amplitude and phase in silicon waveguides with liquid cladding. *Opt. Lett.* **36,** 1869–1871 (2011).
59. Burresi, M. *et al.* Observation of polarization singularities at the nanoscale. *Phys. Rev. Lett.* **102,** 033902 (2009).
60. Veerman, J. A., Garcia-Parajo, M. F., Kuipers, L. & van Hulst, N. F. Single molecule mapping of the optical field distribution of probes for near-field microscopy. *J. Microsc.* **194,** 477–482 (1999).
61. Sick, B., Hecht, B., Wild, U. P. & Novotny, L. Probing confined fields with single molecules and vice versa. *J. Microsc.* **202,** 365–373 (2001).
62. Bauer, T., Orlov, S., Peschel, U., Banzer, P. & Leuchs, G. Nanointerferometric amplitude and phase reconstruction of tightly focused vector beams. *Nature Photon.* **8,** 23–27 (2014).
63. Chicanne, C. *et al.* Imaging the local density of states of optical corrals. *Phys. Rev. Lett.* **88,** 097402 (2002).
64. Lee, K. G. *et al.* Vector field microscopic imaging of light. *Nature Photon.* **1,** 53–56 (2007).
65. Schnell, M., García-Etxarri, A., Alkorta, J., Aizpurua, J. & Hillenbrand, R. Phase-resolved mapping of the near-field vector and polarization state in nanoscale antenna gaps. *Nano Lett.* **10,** 3524–3528 (2010).
66. Rotenberg, N. *et al.* Magnetic and electric response of single subwavelength holes. *Phys. Rev. B* **88,** 241408(R) (2013).
67. Uebel, P., Schmidt, M. A., Lee, H. W. & Russell, P. S. J. Polarisation-resolved near-field mapping of a coupled gold nanowire array. *Opt. Express* **20,** 28409–28417 (2012).
68. Balistreri, M. L. M., Gersen, H., Korterik, J. P., Kuipers, L. & van Hulst, N. F. Tracking femtosecond laser pulses in space and time. *Science* **294,** 1080–1082 (2001).
69. Sandtke, M. & Kuipers, L. Slow guided surface plasmons at telecom frequencies. *Nature Photon.* **1,** 573–576 (2007).
70. Engelen, R. J. P. *et al.* Ultrafast evolution of photonic eigenstates in *k*-space. *Nature Phys.* **3,** 401–405 (2007).
71. Xu, X. G. & Raschke, M. B. Near-field infrared vibrational dynamics and tip-enhanced decoherence. *Nano Lett.* **13,** 1588–1595 (2013).
72. Huth, F., Schnell, M., Wittborn, J., Ocelic, N. & Hillenbrand, R. Infrared-spectroscopic nanoimaging with a thermal source. *Nature Mater.* **10,** 352–356 (2011).
73. Jones, A. C. & Raschke, M. B. Thermal infrared near-field spectroscopy. *Nano Lett.* **12,** 1475–1481 (2012).
74. Amenabar, I. *et al.* Structural analysis and mapping of individual protein complexes by infrared nanospectroscopy. *Nature Commun.* **4,** 2890 (2013).
75. Westermeier, C. *et al.* Sub-micron phase coexistence in small-molecule organic thin films revealed by infrared nano-imaging. *Nature Commun.* **5,** 4101 (2014).
76. Dellinger, J. *et al.* Hyperspectral optical near-field imaging: Looking graded photonic crystals and photonic metamaterials in color. *Appl. Phys. Lett.* **101,** 141108 (2012).
77. Wulf, M., Beggs, D. M., Rotenberg, N. & Kuipers, L. Unravelling nonlinear spectral evolution using nanoscale photonic near-field point-to-point measurements. *Nano Lett.* **13,** 5858–5865 (2013).
78. Shalaev, V. M. Optical negative-index metamaterials. *Nature Photon.* **1,** 41–48 (2007).
79. Denkova, D., Verellen, N., Silhanek, A. V., van Dorpe, P. & Moshchalkov, V. V. Lateral magnetic near-field imaging of plasmonic nanoantennas with increasing complexity. *Small* **10,** 1959–1966 (2014).
80. le Feber, B., Rotenberg, N., van Oosten, D. & Kuipers, L. Modal symmetries at the nanoscale: a route towards a complete vectorial near-field mapping. *Opt. Lett.* **39,** 2802–2805 (2014).
81. Burresi, M. *et al.* Magnetic light–matter interactions in a photonic crystal nanocavity. *Phys. Rev. Lett.* **105,** 123901 (2010).
82. Vignolini, S. *et al.* Magnetic imaging in photonic crystal microcavities. *Phys. Rev. Lett.* **105,** 123902 (2010).
83. Spasenović, M., Beggs, D. M., Lalanne, P., Krauss, T. F. & Kuipers, L. Measuring the spatial extent of individual localized photonic states. *Phys. Rev. B* **86,** 155153 (2012).
84. Huisman, S. R. *et al.* Measurement of a band-edge tail in the density of states of a photonic-crystal waveguide. *Phys. Rev. B* **86,** 155154 (2012).
85. Kihm, H. W. *et al.* Bethe-hole polarization analyser for the magnetic vector of light. *Nature Commun.* **2,** 451 (2011).
86. Kihm, H. W. *et al.* Optical magnetic field mapping using a subwavelength aperture. *Opt. Express* **21,** 5625–5633 (2013).
87. Olmon, R. L. *et al.* Determination of electric-field, magnetic-field, and electric-current distributions of infrared optical antennas: a near-field optical vector network analyzer. *Phys. Rev. Lett.* **105,** 167403 (2010).
88. Grosjean, T. *et al.* Full vectorial imaging of electromagnetic light at subwavelength scale. *Opt. Express* **18,** 5809–5824 (2010).
89. Yang, H. U., Hebestreit, E., Josberger, E. E. & Raschke, M. B. A cryogenic scattering-type scanning near-field optical microscope. *Rev. Sci. Instrum.* **84,** 023701 (2013).
90. Atkin, J. M., Berweger, S., Jones, A. C. & Raschke, M. B. Nano-optical imaging and spectroscopy of order, phases, and domains in complex solids. *Adv. Phys.* **61,** 745–842 (2012).
91. le Feber, B., Rotenberg, N. & Kuipers, L. A scalable interface between solid-state and flying qubits: observations of near-unity dipole helicity to photon pathway coupling. Preprint at http://arxiv.org/abs/1406.7741 (2014).
92. Söllner, I., Mahmoodian, S., Javadi, A. & Lodahl, P. A chiral spin–photon interface for scalable on-chip quantum-information processing. Preprint at http://arxiv.org/abs/1406.4295 (2014).
93. Young, A. B. *et al.* Polarization engineering in photonic crystal waveguides for spin–photon entanglers. Preprint at http://arxiv.org/abs/1406.0714 (2014).
94. Lin, D., Fan, P., Hasman, E. & Brongersma, M. L. Dielectric gradient metasurface optical elements. *Science* **345,** 298–302 (2014).
95. Yu, N. & Capasso, F. Flat optics with designer metasurfaces. *Nature Mater.* **13,** 139–150 (2014).
96. Huth, F. *et al.* Resonant antenna probes for tip-enhanced infrared near-field microscopy. *Nano Lett.* **13,** 1065–1072 (2013).
97. Fang, N., Lee, H., Sun, C. & Zhang, X. Sub-diffraction-limited optical imaging with a silver superlens. *Science* **308,** 534–537 (2005).
98. Novotny, L. & van Hulst, N. Antennas for light. *Nature Photon.* **5,** 83–90 (2011).
99. Okamoto, K. *Fundamentals of Optical Waveguides* (Academic, 2005).
100. Baba, T. Slow light in photonic crystals. *Nature Photon.* **2,** 465–473 (2008).
101. Johnson, S. G. & Joannopoulos, J. D. Block-iterative frequency-domain methods for Maxwell's equations in a planewave basis. *Opt. Express* **8,** 173–190 (2001).

Acknowledgements

We thank B. le Feber for discussions and help in the preparation of this manuscript, and A. de Hoogh for help with the figures. This work is part of the research programme of the Foundation for Fundamental Research on Matter (FOM), which is part of the Netherlands Organisation for Scientific Research (NWO). This work is supported by the EU FET project "SPANGL4Q" and was also funded by ERC Advanced Investigator Grant (no. 240438-CONSTANS).

Additional information

Reprints and permissions information is available online at www.nature.com/reprints. Correspondence should be addressed to L.K.

Competing financial interests

The authors declare no competing financial interests.